


Electrically driven nematic flow in microfluidic capillary with radial temperature gradient

A. V. Zakharov*

*Saint Petersburg Institute for Machine Sciences, The Russian Academy of Sciences, Saint Petersburg 199178, Russia*P. V. Maslennikov[†]*Immanuel Kant Baltic Federal University, Kaliningrad 236040, Str. Universitetskaya 2, Russia*S. V. Pasechnik[‡]*Russian Technological University (MIREA), Moscow 119454, Russia* (Received 7 September 2020; revised 24 November 2020; accepted 1 January 2021; published 13 January 2021)

An electrically driven fluid pumping principle and a mechanism of kinklike distortion of the director field $\hat{\mathbf{n}}$ in the microsized nematic volume has been described. It is shown that the interactions, on the one hand, between the electric field \mathbf{E} and the gradient of the director's field $\nabla\hat{\mathbf{n}}$, and, on the other hand, between the $\nabla\hat{\mathbf{n}}$ and the temperature gradient ∇T arising in a homogeneously aligned liquid crystal microfluidic channel, confined between two infinitely long horizontal coaxial cylinders, may excite the kinklike distortion wave spreading along normal to both cylindrical boundaries. Calculations show that the resemblance to the kinklike distortion wave depends on the value of radially applied electric field \mathbf{E} and the curvature of these boundaries. Calculations also show that there exists a range of parameter values (voltage and curvature of the inner cylinder) producing a nonstandard pumping regime with maximum flow near the hot cylinder in the horizontal direction.

DOI: [10.1103/PhysRevE.103.012702](https://doi.org/10.1103/PhysRevE.103.012702)**I. INTRODUCTION**

The problem of electrically driven manipulation of biomolecules and biosensing has brought an increasing number of integrated small-scaled microdevices for chemical and biological applications [1–4]. The confinement of a fluid between walls separated on the micron scale can impose significant conditions on the flow behavior of the material [5,6]. Manipulation of complex liquids such as liquid crystals (LCs) can be achieved either by forces applied macroscopically [7], or can be generated locally within the microfluidic channel or liquid crystal (LC) capillary [8,9]. Electro-osmosis, dielectrophoresis, and electrowetting have been explored for controlling microflows [2,9,10]. Thus, understanding the flow of liquid crystals through micron-scale channels is of increasing significance. Nematic liquid crystal (NLC) channels and capillaries of appropriate size are microdevices, whose molecular orientations can be manipulated by the presence of electric field \mathbf{E} and the temperature gradient ∇T [5,6]. A challenging problem in all such systems is the precise handling of LC or anisotropic liquid microvolume [5], which in turn requires self-contained micropumps of small package size exhibiting either a very small displacement volume (displacement pumps) or a continuous volume flow (dynamic pumps). One of the liquid crystal pumping principles is based on the coupling between the electric and director fields, to-

gether with accounting the effect of the temperature gradient ∇T [5,6]. In this case, the uniform textures of nematic LCs are produced by orienting a drop of bulk material in-between two conveniently treated bounding surfaces, which define usually a fixed orientation for the boundary molecules. When there is no temperature gradient, the electric field \mathbf{E} applying perpendicular to a uniformly (homogeneously) oriented NLC can distort the molecular orientation $\hat{\mathbf{a}}$ with respect to director $\hat{\mathbf{n}}$, at a critical threshold field E_{th} given by [11] $E_{\text{th}} = \frac{\pi}{d} \sqrt{\frac{K_1}{\epsilon_0 \epsilon_a}}$, where d is the thickness of the microsized LC channel, K_1 is the splay elastic constant, ϵ_0 is the absolute dielectric permittivity of free space, ϵ_a is the dielectric anisotropy of the NLC. This form for the critical field is based upon the assumption that the director remains strongly anchored (in our case, homogeneously) at the two horizontal bounding surfaces and that the physical properties of the LC are uniform over the entire sample for $E < E_{\text{th}}$. When the electric field is switched on with a magnitude E greater than E_{th} , the director $\hat{\mathbf{n}}$, in the “splay” geometry, reorients as a simple monodomain [12], and exciting of the electrically driven nematic flow in microfluidic channel containing a temperature gradient is a question of great fundamental interest, as well as an essential piece of knowledge in soft material science [1]. In the nematic microfluidic channel where director anchoring on the bounding surfaces is the same, i.e., both homogeneous, and when the gradient of the temperature field ∇T does not exist, the horizontal flow of the nematic material is excited only by the electric field $\mathbf{E} = E(z)\hat{\mathbf{k}}$ directed orthogonally to the homogeneously aligned LC sample. In turn, accounting the temperature gradient ∇T , generated, for instance, by the uniform heating both from below or above, leads to the

* Author to whom correspondence should be addressed: alexandre.zakharov@yahoo.ca; homepage: www.ipme.ru[†] pashamaslennikov@mail.ru[‡] s-p-a-s-m@mail.ru

additional contributions to the torque and linear momentum balance equations [6].

In this study we explore a high curvature of microsized cylinder cavity and consider the joint effect of flexoelectric polarization and thermomechanical flow on director reorientation and steady flow in the LC system. Flexoelectric coupling and dielectric anisotropy are taken into account in the pumping model, together with a temperature difference $\Delta T = T_2 - T_1 > 0$ across the nematic cavity, where the range $[T_1, T_2]$ still falls within the stability region of the nematic phase. The new additional vector field $\mathbf{P} = e_1 \hat{\mathbf{n}}(\nabla \cdot \hat{\mathbf{n}}) + e_3(\nabla \times \hat{\mathbf{n}}) \times \hat{\mathbf{n}}$, where e_i ($i = 1, 3$) denote the flexoelectric coefficients [13], keeps the null property of the distortion of the microsized nematic cavity, when no voltage is applied and the director anchorings on the two bounding surfaces are the same, i.e., both strongly homeotropic or both homogeneous, and the microvolume remains quiescent under the influence of the temperature gradient [6]. The voltage applied across the homogeneously aligned liquid crystal (HALC) cavity makes backflow possible in the microvolume, and backflow is additionally influenced by \mathbf{P} . A heating of the nematic cavity ($\Delta T \neq 0$) causes flexoelectric and thermomechanical couplings; their intercorrelation solves the problem of establishing a steady horizontal flow in the microsized nematic volume.

Here, we focus, on the one hand, on the description of a mechanism of the kinklike distortion wave of the director field $\hat{\mathbf{n}}$ in the microsized nematic volume under the effect of voltage U applied between two cylinders and a temperature gradient ∇T , which is set up between cooler inner and hotter outer cylinders. It is found that, under certain conditions, in terms of curvature of cylinders κ and the voltage U , applied between cylinders, the torques and forces acting on the director $\hat{\mathbf{n}}$ may excite the kinklike distortion wave spreading along the normal to both cylindrical boundaries, whose resemblance to a kinklike distortion wave depends on the value of U and the curvature of the inner cylinder. It has been worked out, on the other hand, the conditions, in terms of κ and U , producing the distortion mechanism of the $\hat{\mathbf{n}}$ in the double π form, with the intermediate relaxation wall.

We assumed that the relaxation behavior of the director field $\hat{\mathbf{n}}$ in the form of the kinklike distortion wave spreading along the normal to both cylindrical boundaries probably can be observed in polarized white light. Taking into account that under certain voltage applied across the nematic cavity with $\Delta T = T_{\text{out}} - T_{\text{in}} > 0$, the director reorientation takes place in the running narrow area of the LC sample (the width of the kinklike distortion wave). This kinklike distortion wave can be visualized in polarized white light as a dark strip running along the normal to both cylindrical boundaries, with the velocity in a few tens of $\mu\text{m/s}$. This dark running strip can be recorded using a charge-coupled-device camera and video cassette recorder, while the temperature difference, for the experimentally well studied and technologically interesting case of 4-n-pentil-4'-cyanobiphenyl (5CB) can be achieved by pumping the cooling material (with a temperature T_{in} less than with 5° below room temperature T_{out}) through the inner cylinder.

The aim of our paper is to analyze the response of a homogeneously aligned liquid crystal microsized cavity confined

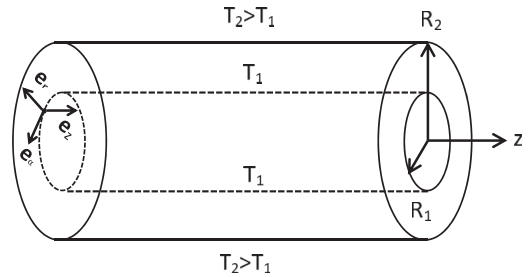


FIG. 1. Geometry of a homogeneously aligned liquid crystal (LC) capillary. The z axis and the unit vector $\hat{\mathbf{e}}_z$ are taken as being parallel to coaxial cylinders which are kept at different temperatures, with the outer one $T_{r=R_2} = T_2$ hotter than the inner one $T_{r=R_1} = T_1$ ($T_2 > T_1$). The cylinder LC cavity $d = R_2 - R_1$ confined between two infinitely long horizontal coaxial cylinders is subjected to both radially applied temperature gradient ∇T and electric field $\mathbf{E} = E(r)\hat{\mathbf{e}}_r$.

between two horizontal coaxial cylinders and subjected to both a temperature gradient ∇T , which is set up between cooler inner and hotter outer cylinders, and a voltage U applied between these cylinders. This problem will be treated in the framework of the classical Ericksen-Leslie theory [14,15], supplemented by the thermomechanical correction of shear stress [6] and the thermoconductivity equation for the temperature field [16]. This paper is organized as follows: the relevant equations describing director motion, fluid flow, and temperature distribution in the above named system are given in Sec. II; numerical results for different possible relaxation regimes are given in Sec. III; conclusions are summarized in Sec. IV.

II. FORMULATION OF THE BASIC EQUATIONS FOR MICROFLUIDIC CAPILLARY

We are primarily concerned with the description of the physical mechanism responsible for the electrically driven nematic flow in microfluidic homogeneously aligned liquid crystal (HALC) capillary containing a temperature gradient ∇T . This gradient was fixed between two infinitely long horizontal coaxial cylinders which are kept at different temperatures, with the outer one $T_{r=R_2} = T_{\text{out}} = T_2$ hotter than the inner one $T_{r=R_1} = T_{\text{in}} = T_1$ ($T_2 > T_1$). In this study we explore a cylindrical nematic cavity with radii R_1 and R_2 , where $R_1 < R_2$ and $d = R_2 - R_1$ is the capillary thickness (see Fig. 1). We shall be using the corresponding dimensionless radii $a = \frac{R_1}{d}$ and $a + 1$, and assume the dimensionless curvature values $\kappa = \frac{1}{a}$. So, one deals with the HALC system composed of asymmetric polar molecules, such as *cyanobiphenyls*, at the density ρ , and confined between two horizontal coaxial cylinders which are kept at different temperatures $\chi_{\text{in}} = \chi_1$ and $\chi_{\text{out}} = \chi_2$ ($\chi_1 < \chi_2$), where both dimensionless temperatures are scaled by the nematic-isotropic transition value, i.e., $\chi_i = \frac{T_i}{T_{\text{NI}}}$ ($i = 1, 2$), and subjected to both radially applied temperature gradient $\nabla \chi = \chi_{,r}(r)\hat{\mathbf{e}}_r$ and electric field $\mathbf{E} = E(r)\hat{\mathbf{e}}_r$. Here, $\chi_{,r} = \partial \chi / \partial r$ denotes the partial derivative of temperature χ with respect to space coordinate r and $\hat{\mathbf{e}}_r$ is the unit vector along the dimensionless radius r (i.e., scaled by d). The other unit vectors of the cylindrical coordinate

system to be used here are $\hat{\mathbf{e}}_z$, defined by the common axis of the two cylinders, and the tangential one $\hat{\mathbf{e}}_\alpha = \hat{\mathbf{e}}_z \times \hat{\mathbf{e}}_r$. The voltage U applied between two horizontal coaxial cylinders can be scaled by the threshold value for producing the distortion (Freederickz voltage), i.e., $U = U_0 U_{\text{th}}$, with U_{th} defined by $U_{\text{th}} = \pi \sqrt{\frac{K_1}{\epsilon_0 \epsilon_a}}$; here $\epsilon_a = \epsilon_{\parallel} - \epsilon_{\perp}$ denotes the nematic dielectric anisotropy, defined by the difference between (dimensionless) dielectric constants along and perpendicular to the director $\hat{\mathbf{n}}$ [11].

Assuming both that the temperature gradient $\nabla \chi$ and the electric field \mathbf{E} vary only in the r direction and the LC molecules are confined between two coaxial cylinders with the planar preferred orientation of the average molecular direction $\hat{\mathbf{n}}_{r=a} \parallel \hat{\mathbf{e}}_z$ ($\hat{\mathbf{n}}_{r=a+1} \parallel \hat{\mathbf{e}}_z$) on the bounding surfaces, we can suppose that the components of the director $\hat{\mathbf{n}} = n_r \hat{\mathbf{e}}_r + n_z \hat{\mathbf{e}}_z$, as well as the rest of the physical quantities also depend only on the coordinate r , and the coordinate system defined by our task entails that the director $\hat{\mathbf{n}}$ lies in the rz plane.

Taking into account the microized volume of the LC cavity, one can assume the mass density ρ to be constant over the LC volume, and thus we can deal with an incompressible fluid. The incompressibility condition $\nabla \cdot \mathbf{v} = 0$ assumes that only one nonzero component of the vector \mathbf{v} exists, viz., $\mathbf{v}(r, \tau) = v_z(r, \tau) \hat{\mathbf{e}}_z = u(r, \tau) \hat{\mathbf{e}}_z$. So, we are primarily concerned here with describing the way how both the temperature gradient and electric field across the microvolume cavity between two coaxial cylinders can produce the hydrodynamic quasi-two-dimensional (quasi-2D) flow $v_z(r, \tau)$.

The condition for producing a distortion of the nematic microvolume is $U_0 > 1$, which inputs the electric field component $E(r)$ self-consistently with the nematic distortion $\nabla \hat{\mathbf{n}}$ [17]. We will assume homogeneous strong anchoring of the director on both bounding cylindrical surfaces, i.e.,

$$n_r(r)_{r=a} = n_r(r)_{r=a+1} = 0, \quad (1)$$

together with the no-slip conditions

$$u(r)_{r=a} = u(r)_{r=a+1} = 0, \quad (2)$$

where u denotes the dimensionless component of horizontal velocity v_z of the incompressible liquid crystal. Notice that the normalization of the velocity component v_z is defined by U_0 and by the time scaling $\frac{1}{(\pi U_0)^2} \frac{\gamma_1 d^2}{K_1}$, so that $u = \left(\frac{\gamma_1 d}{K_1}\right) \frac{1}{(\pi U_0)^2} v_z$, where γ_1 denotes the rotational viscosity coefficient, taken at the temperature χ_1 . The boundary conditions on temperature are reduced to

$$\chi(r)_{r=a} = \chi_1, \quad \chi(r)_{r=a+1} = \chi_2. \quad (3)$$

In the nematic phase, splay and bend deformations, caused by electric field, give rise to two independent flexoelectric coefficients (e_1, e_3). Their contributions to induced polarization can be written as $\mathbf{P} = P_r \hat{\mathbf{e}}_r + P_z \hat{\mathbf{e}}_z$, where the vector components are given by the classical Meyer model [13]

$$P_r = \delta_1 \left[\left(1 + \frac{e_3}{e_1} \right) n_r n_{r,r} + \frac{n_r^2}{r} \right] \quad (4)$$

and

$$P_z = \delta_1 \left[n_z \nabla_{,r} n_r + \frac{e_3}{e_1} n_r n_{z,r} \right], \quad (5)$$

where $\delta_1 = \frac{e_1}{U_0 \sqrt{K_1 \epsilon_0 \epsilon_a}}$ is a dimensionless parameter, $n_{i,r} = \frac{\partial n_i}{\partial r}$ ($i = r, z$) denote the partial derivative of director components with respect to space coordinate, and $\nabla_{,r}(\dots) = (\dots)_{,r} + \frac{n_r}{r}$ is a divergence.

The flexoelectric radial component [Eq. (4)] leads to the dimensionless charge balance [17]

$$\nabla_{,r} \left[E(r) \left(\frac{\epsilon_{\perp}}{\epsilon_a} + n_r^2 \right) + P_r \right] = 0, \quad (6)$$

which has the solution

$$E = \frac{\mathcal{A} - r P_r}{r \left(\frac{\epsilon_{\perp}}{\epsilon_a} + n_r^2 \right)}, \quad (7)$$

with $\mathcal{A} = \frac{\mathcal{A}_p}{\mathcal{A}_E}$, $\mathcal{A}_p = 1 + \int_a^{a+1} \frac{P_r dr}{r \left(\frac{\epsilon_{\perp}}{\epsilon_a} + n_r^2 \right)}$, $\mathcal{A}_E = \int_a^{a+1} \frac{dr}{r \left(\frac{\epsilon_{\perp}}{\epsilon_a} + n_r^2 \right)}$ following from the condition of electric field normalization $\int_a^{a+1} E(r) dr = 1$. The reorientation process in the HALC cavity, excited by both $\Delta \chi = \chi_2 - \chi_1$ and U_0 , entails time dependence of the director $\hat{\mathbf{n}} = \hat{\mathbf{n}}(r, \tau)$, where the dimensionless time $\tau = (\pi U_0)^2 \frac{K_1}{\gamma_1 d^2} t$ includes the orientational relaxation time $\frac{t K_1}{\gamma_1 d^2}$. Owing to director dynamics, the static fields $\mathbf{P}(r)$ and $E(r)$ [Eqs. (4), (5), and (7)] actually take the quasistatic forms $E = E(r, \tau)$, $\mathbf{P} = \mathbf{P}(r, \tau)$.

Upon assuming an incompressible fluid ($\rho = \text{const}$), the hydrodynamic equations describing the reorientation of the homogeneously aligned nematic system in the named setting can be derived from the balance of electric, flexoelectric, elastic, viscous, and thermomechanical torques, coupled with Navier-Stokes equation for the velocity field $\mathbf{u} = u(r, \tau) \hat{\mathbf{e}}_z$, and the equation for heat conduction.

In the present coordinate system, the dimensionless torque balance equation reads as (for details, see the Appendix)

$$\left[\frac{\delta \mathcal{W}_F}{\delta \hat{\mathbf{n}}} - \frac{\delta \psi^{\text{el}}}{\delta \hat{\mathbf{n}}} + \frac{\delta \mathcal{R}}{\delta \hat{\mathbf{n}}} \right] \times \hat{\mathbf{n}} = 0, \quad (8)$$

where $2\mathcal{W}_F = K_1 n_{r,r}^2 + K_3 n_{z,r}^2$ is the elastic, $2\psi^{\text{el}} = \epsilon_0 (\epsilon_{\perp} + \epsilon_a n_r^2) E^2(r) + 2P_r E(r)$ is the electric torque, whereas $\mathcal{R} = \mathcal{R}_{\text{vis}} + \mathcal{R}_{\text{tm}} + \mathcal{R}_{\text{th}}$ is the full Rayleigh dissipation function composed by viscous, thermomechanical, and thermal contributions, respectively. All torques have the tangential component only, and have been normalized by the value $(\pi U_0)^2 \frac{K_1}{d^2}$. The torque components can thus be written as

$$T_{\text{el}} = E^2(r, \tau) n_r n_z, \quad (9)$$

$$T_p = E(r, \tau) P_z(r, \tau), \quad (10)$$

$$T_{\text{elast}} = \frac{1}{(\pi U_0)^2} \left[\mathcal{K}_{,r} + \frac{1}{r} \mathcal{K} - (1 - K_{31}) n_{z,r}^2 - \frac{1}{r^2} n_r n_z \right], \quad (11)$$

for electric, flexoelectric, and elastic torques, respectively. Here, $\mathcal{K} = n_z n_{r,r} - K_{31} n_r n_{z,r}$, $K_{31} = K_3/K_1$, K_3 is the bend elastic constant, and the viscous and thermomechanical torques are defined by the dissipative process in the HALC and follow from the dimensionless dissipative function $\mathcal{R} = \mathcal{R}_{\text{vis}} + \frac{\delta_2}{(\pi U_0)^2} \mathcal{R}_{\text{tm}} + \frac{\delta_3}{(\pi U_0)^4} \mathcal{R}_{\text{th}}$. Here, $\delta_2 = \frac{\xi T_{\text{NI}}}{K_1}$ and $\delta_3 = \frac{\lambda_{\perp} T_{\text{NI}} \gamma_1 d^2}{K_1^2}$ are additional parameters of the LC system, λ_{\perp} is the

heat conductivity coefficient perpendicular to the director, and γ_1 denotes the rotational viscosity coefficient, respectively.

In order to evaluate the order of parameters δ_i ($i = 1, 2, 3$), one can take $d \sim 50 \mu\text{m}$ in the HALC capillary, whereas the value of density ρ was chosen to be equal to 10^3 kg/m^3 . The value of the heat conductivity λ_\perp was chosen to be equal to 0.24 W/mK [18], both the Frank elastic coefficients K_1 and K_3 were chosen as $\sim 10 \text{ pN}$ and $\sim 13.8 \text{ pN}$ [19], respectively, both the RVCs γ_1 and γ_2 were chosen as $\sim 0.071 \text{ Pa s}$ and $\sim -0.079 \text{ Pa s}$ [20], respectively, the value of the specific heat C_p is equal to 10^3 J/kg K [21], and finally the values of the flexoelectric coefficients e_1 and e_3 were chosen to be equal to -11.6 and 4.3 pC/m [22], respectively. Then, δ_2 and δ_3 can be estimated as ~ 30.7 and $\sim 1.3 \times 10^{14}$, whereas $\delta_1 \sim -0.065$, at $U_0 = 6$, and $\delta_1 \sim -0.026$, at $U_0 = 14$, respectively. The reorientational dissipation process is described by the viscous dissipation function \mathcal{R}_{vis} (the Ericksen-Leslie dissipation function [14,15,23]), where the thermomechanical part \mathcal{R}_{tm} acts as additional term, whereas the thermal part of the dissipation function \mathcal{R}_{th} controls the heat conduction process, where the input of \mathcal{R}_{tm} is negligible. The \mathcal{R} function is most sensitive to the increasing of the voltage U_0 . If one takes, for instance, $U_0 > 20$, then the \mathcal{R}_{tm} term, due to the factor $\frac{\delta_2}{(\pi U_0)^2}$, does not play any role in the dissipation process for the HALC under study. In the further calculations the values U_0 are constrained to be $U_0 \leq 20$, and cause the radial gradient u_r of horizontal velocity, rotation rate of director $\dot{\mathbf{n}}$, and temperature gradient $\chi_{,r}$ interactions supplemented by the flexoelectric polarization. The viscous and thermomechanical torque components can thus be written as

$$T_{\text{vis}} = n_r \dot{n}_z - n_z \dot{n}_r - \frac{1}{2} u_{,r} [1 - \gamma_{21} (n_z^2 - n_r^2)] \quad (12)$$

and

$$T_{\text{tm}} = \frac{1}{2} \frac{\delta_2}{(\pi U_0)^2} \chi_{,r} [n_z n_{r,r} (3 + n_r^2) - n_r n_{z,r} (1 + n_r^2)], \quad (13)$$

respectively. Here, $\gamma_{21} = \gamma_2/\gamma_1$, and $\dot{n}_i = \frac{\partial n_i}{\partial \tau}$ ($i = r, z$) is the partial derivative with respect to time.

The dimensionless Navier-Stokes equation (in cylindrical coordinates) takes the form [24]

$$\delta_4 (\pi U_0)^2 \dot{u} = \nabla_{,r} [\sigma_{rz}^{\text{vis}} + \sigma_{rz}^{\text{tm}}], \quad (14)$$

$$\nabla_{,r} \sigma_{rr}^{\text{elast}} - \frac{\sigma_{\alpha\alpha}^{\text{elast}}}{r} + \psi_{,r}^{\text{el}} = 0, \quad (15)$$

where $\delta_4 = \frac{\rho K_1}{\gamma_1^2}$ is an additional parameter of the system. Here, $\sigma_{rr}^{\text{elast}} = -\frac{1}{(\pi U_0)^2} [Q(r) + (n_{r,r} + \frac{n_r}{r}) n_{r,r} + \frac{K_3}{K_1} n_{z,r}^2]$ and $\sigma_{\alpha\alpha}^{\text{elast}} = -\frac{1}{(\pi U_0)^2} [Q(r) + (n_{r,r} + \frac{n_r}{r}) \frac{n_r}{r}]$ are the two normal ST components, $Q(r)$ is the dimensionless hydrodynamic pressure, and $2\psi^{\text{el}} = \epsilon_0 (\epsilon_\perp + \epsilon_a n_r^2) E^2(r) + 2P_r E(r)$ is the electric energy density. The shear stress component has the viscous and thermomechanical terms $\sigma_{rz}^{\text{vis}} = \frac{\delta \mathcal{R}_{\text{vis}}}{\delta u_{,r}}$ and $\sigma_{rz}^{\text{tm}} = \frac{\delta \mathcal{R}_{\text{tm}}}{\delta u_{,r}}$. The Ericksen-Leslie form for the viscous part of dissipation function [14,15,23,24] gives the shear stress component for the geometry under consideration

$$\sigma_{rz}^{\text{vis}} = \frac{1}{2} (n_z \dot{n}_r - n_r \dot{n}_z) + \gamma_{21} (n_z^2 - n_r^2) + h u_{,r}, \quad (16)$$

and the thermomechanical part of shear stress [6]

$$\sigma_{rz}^{\text{tm}} = \frac{1}{4} \frac{\delta_1}{(\pi U_0)^2} \chi_{,r} [n_r n_z (1 + 2n_r^2) + 6n_z n_{r,r} - n_r^3 n_{z,r}], \quad (17)$$

where $h = [\alpha_4 + \frac{1}{2}(\gamma_1 + \alpha_5 + \alpha_6) + \alpha_1 n_r^2 n_z^2 + \gamma_2 (n_z^2 - n_r^2)]/\gamma_1 = \mathcal{H}/\gamma_1$ is the dimensionless hydrodynamic function, and α_i ($i = 1-6$) denote the Leslie viscous coefficients, respectively. When a small mean temperature gradient (in our case $\sim 1 \text{ K}/\mu\text{m}$) is set up across the system, we expect the temperature field $\chi(r, \tau)$ to satisfy the dimensionless heat conduction equation [16]

$$\delta_5 \dot{\chi} = \left(\frac{1}{\pi U_0} \right)^2 \frac{1}{r} [r \chi_{,r} (\lambda n_r^2 + n_z^2)]_{,r}, \quad (18)$$

where $\lambda = \frac{\lambda_\parallel}{\lambda_\perp}$ is the ratio of heat conductivity coefficients along and perpendicular to the director, $\delta_5 = \frac{\rho C_p K_1}{\lambda_\perp \gamma_1}$ is another parameter of the system, and C_p denotes the heat capacity. Notice that our approach is only valid for the nematic phase; notice also that various material parameters have been mentioned so far, and that numerical values have to be used for them: we have thus chosen the experimentally well studied and technologically interesting case of 4-n-pentyl-4'-cyanobiphenyl (5CB); at temperature corresponding to the nematic phase, the parameter values involved in Eqs. (8), (14), and (18) are $\delta_1 \sim -0.07$, at $U_0 = 6$, and $\delta_1 \sim -0.026$, at $U_0 = 14$, respectively, $\delta_2 \sim 30.7$, $\delta_3 \sim 1.3 \times 10^{14}$, $\delta_4 \sim 2 \times 10^{-6}$, $\delta_5 \sim 6.0 \times 10^{-4}$. Using the fact that δ_4, δ_5 are $\ll 1$, both the Navier-Stokes [Eq. (14)] and the heat conduction [Eq. (18)] equations can be simplified and reduced to

$$\sigma_{rz}^{\text{vis}} + \sigma_{rz}^{\text{tm}} = \frac{\mathcal{C}}{r}, \quad (19)$$

$$\chi(r, \tau) = \frac{\chi_2 - \chi_1}{\mathcal{I}} \int_a^r \frac{dr}{r(\lambda n_r^2 + n_z^2)} + \chi_1, \quad (20)$$

where the function $\mathcal{C}(\tau)$ do not depend on r and will be fixed by the boundary condition (2), and $\mathcal{I}(\tau) = \int_a^{a+1} \frac{dr}{r(\lambda n_r^2 + n_z^2)}$. The smallest initial perturbation of the director component $n_r(r, \tau_0)$ gives the initial values $A(\tau_0)$, $\mathcal{I}(\tau_0)$, defined by the electric normalization condition and the boundary conditions (3). Equation (15) can be used here for defining the pressure $Q(r)$, and has the solution

$$Q(r, \tau) = \psi^{\text{el}} + \sigma_{rr}^{\text{elast}} + \int_0^r \frac{\sigma_{rr}^{\text{elast}} - \sigma_{\alpha\alpha}^{\text{elast}}}{r} dr + Q_0, \quad (21)$$

where Q_0 is an arbitrary constant. As for numerical solution of the above equations (8), (19), and (20), the torque values $T_{\text{el}}(r, \tau_0)$, $T_P(r, \tau_0)$, $T_{\text{elast}}(r, \tau_0)$, and $T_{\text{tm}}(r, \tau_0)$ can be calculated by the corresponding cases in Eqs. (9), (10), (11), and (13); the director rotation rate is eliminated from the system of equations by means of Eqs. (8), (14), and the value $\mathcal{C}(\tau_0)$ can be found using the boundary conditions (1) and (2). The initial velocity gradient $u_r(r, \tau_0)$ from Eqs. (19) and (20) yields the director component distribution $n_r(r, \tau_0 + \Delta\tau)$ from Eq. (8), and the procedure is iterated up to the stationary state of $n_r^{\text{eq}}(r)$, which imposes the stationary distributions of velocity $u^{\text{eq}}(r)$ and temperature $\chi^{\text{eq}}(r)$. The thermodynamic

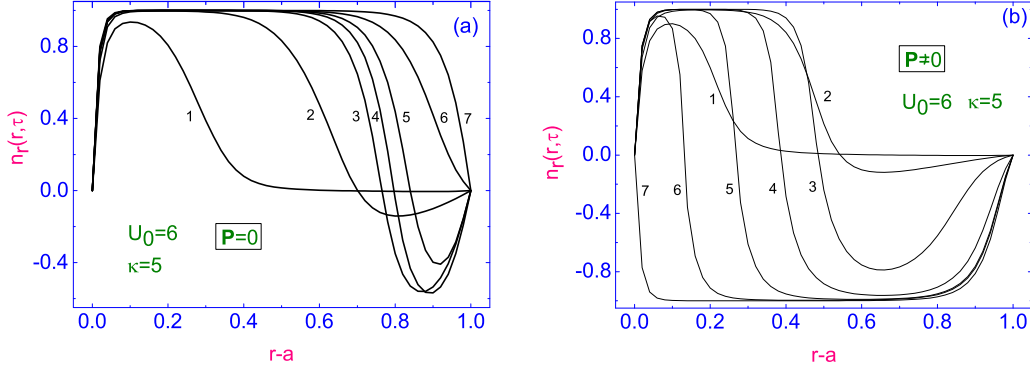


FIG. 2. Plot of the evolution of the director's field component $n_r(r, \tau_i)$, for different times $\tau_i = 0.01i$ ($i = 1, \dots, 7$) [$\tau_7 = \tau_R$ ($t_R \sim 50$ ms)], to its equilibrium distribution $n_r^{\text{eq}}(r, \tau_7) \equiv n_r^{\text{eq}}(r)$ across the microsized HALC cavity $a \leq r \leq a + 1$, under the effect of the electric field $U_0 = 6$ and the temperature difference $\Delta\chi = 0.0162$, both for the cases $\mathbf{P} = \mathbf{0}$ (a) and $\mathbf{P} \neq \mathbf{0}$ (b), respectively. Here, $\kappa = 5$.

condition $\dot{\mathcal{R}}_{\text{full}} < 0$, $\mathcal{R}_{\text{full}} = \int_a^{a+1} \mathcal{R} dr$ [25] yields a check on convergence.

III. NUMERICAL RESULTS

The system of nonlinear partial differential equations (8), (19) and (20), together with the boundary conditions (1) to (3) and the initial condition $n_r = 0.001$ ($a < r < a + 1$), has been solved by the numerical relaxation method [26]. Each calculation has been repeated both for the case involving no flexoelectrical polarization, defined by setting $\mathbf{P} = \mathbf{0}$ [see the curves shown on the left-hand side in Figs. 2(a) to 3(a)] and for the case with accounting the flexoelectrical polarization $\mathbf{P} \neq \mathbf{0}$ [see the curves shown on the right-hand side in Figs. 2(b) to 3(b)] throughout the relevant equations. Calculations for both models use the relaxation criterion $\epsilon = |(n_r(r, \tau_{m+1}) - n_r(r, \tau_m)) / n_r(r, \tau_m)|$ with $\epsilon = 10^{-4}$, and the numerical procedure was then carried out until a prescribed accuracy was achieved. Here, m denotes the iteration number. The set of external parameters were chosen as $\kappa \in (1, 10]$, $U_0 \in (1, 20]$ and the temperature difference for the cold-hot heating system was fixed by $\chi_1 = 0.97$ and $\chi_2 = 0.9862$, respectively. The ratios of other main physical parameters were fixed to $\frac{\epsilon_{\perp}}{\epsilon_a} = 0.8$, $\frac{\epsilon_3}{\epsilon_1} = -0.37$, and $\lambda = 2$.

Figures 2 and 3 show the evolution of the director's field component $n_r(r, \tau)$ to its equilibrium distribution $n_r^{\text{eq}}(r, \tau_R) \equiv$

$n_r^{\text{eq}}(r)$ across the microsized HALC cavity $a \leq r \leq a + 1$, calculated for two voltages $U_0 = 6$ (see Fig. 2) and 14 (see Fig. 3), and fixed curvature $\kappa = 5$ ($a = 0.2$).

The distributions $n_r(r, \tau)$ are plotted versus $r - a$ for different τ , where $\tau_i = 0.01i$ ($i = 1, \dots, 7$), for the case $U_0 = 6$ [Figs. 2(a) and 2(b)], whereas $\tau_i = 0.0005i$ ($i = 1, \dots, 10$) [Figs. 3(a) and 3(b)], for the case $U_0 = 14$, respectively. The equilibrium states have been established in the HALC cavity at times $\tau_R = \tau_7$ ($t_R \sim 50$ ms) for $U_0 = 6$, and $\tau_R = \tau_{10}$ ($t_R \sim 50$ μ s) for $U_0 = 14$, respectively. Figures 2(b) and 3(b) show the most pronounced effect of flexoelectricity on the orientational dynamics. The torques \mathbf{T}_P , \mathbf{T}_{tm} produce a kinklike reorientation of the director [curves from 4 to 6 in Fig. 2(b)]. This process shows an initial stage, where the electric torque near the inner cylinder $r = a$, over the period $\tau < \tau_1$, perturbs the director distortion. At that time the sum of the torques [Eqs. (10) and (13)] $\mathbf{T}_P + \mathbf{T}_{\text{tm}}$ acts in opposite verse near the outer cylinder $r = a + 1$. The values of the radial director component have become negative and the kinklike reorientation is building up [Fig. 2(b) solid curves 2 and 3], during the time interval $\tau_1 < \tau < \tau_3$, under the increasing flexoelectric torque. The field $E(r, \tau)$ is strong and the sum of torques $\mathbf{T}_P + \mathbf{T}_{\text{tm}}$ continues the process of kink motion towards the inner cylinder [Fig. 2(b), curves 4, 5, and 6]. Due to the nematic symmetry, the stationary distributions of $n_r^{\text{eq}}(r)$ [curve 7 in

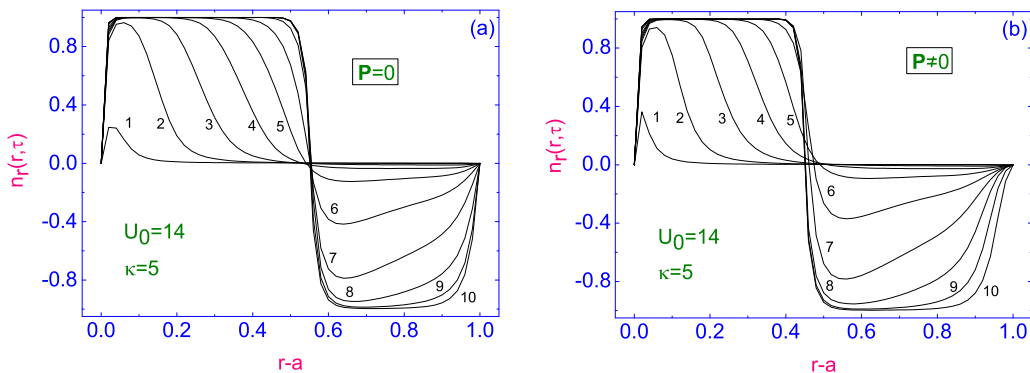


FIG. 3. Plot of the evolution of the director's field component $n_r(r, \tau_i)$, for different times $\tau_i = 0.0005i$ ($i = 1, \dots, 10$) ($\tau_{10} = \tau_R$) ($t_R \sim 50$ μ s), to its equilibrium distribution $n_r^{\text{eq}}(r, \tau_{10}) \equiv n_r^{\text{eq}}(r)$ across the microsized HALC cavity $a \leq r \leq a + 1$, under the effect of the electric field $U_0 = 14$ and the temperature difference $\Delta\chi = 0.0162$. Here, $\kappa = 5$.

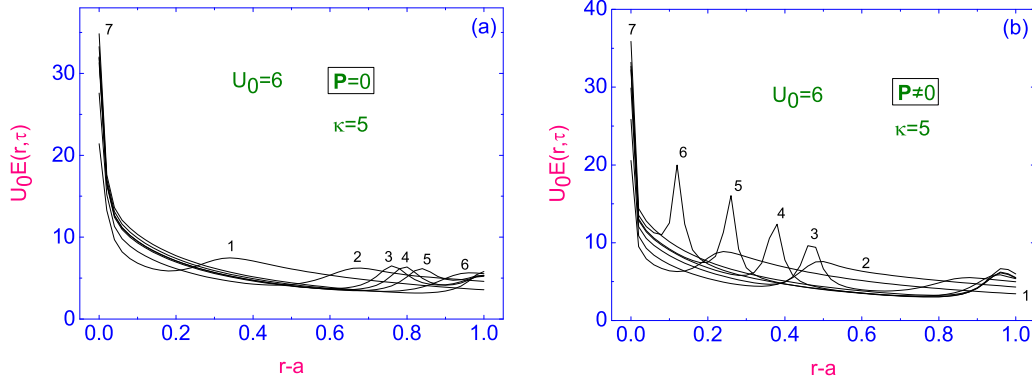


FIG. 4. Same as described in the caption of Fig. 2, but a plot of the evolution of the electric field $U_0 E(r, \tau_i)$ to its equilibrium distribution $U_0 E^{\text{eq}}(r, \tau_7) \equiv U_0 E^{\text{eq}}(r)$ across the microsized HALC cavity $a \leq r \leq a + 1$, both for the cases $\mathbf{P} = \mathbf{0}$ (a) and $\mathbf{P} \neq \mathbf{0}$ (b), respectively. Here, $U_0 = 6$.

Fig. 2(a) and $n_r^{\text{eq}}(r)$ [curve 7 in Fig. 2(b)] are equivalent, the relaxation times of two models are close to each other, but their relaxation ways to the stationary states are different.

Results for the model of $\mathbf{P} = \mathbf{0}$ show that the torque \mathbf{T}_{tm} tends to perturb the director component n_r , but it is not strong enough to produce the kinklike distortion of the director profile [Fig. 2(a), curves 3 to 6]. This slow reconstruction of the orientation profile by the viscous torque is similar to the slow orientational dynamics reported in [27]. The kink evolution, shown in Fig. 2(b) (curves 4, 5, and 6), correlates with the electric field function $E(r, \tau)$ [Fig. 4(b)]. The local maximum points of $E(r, \tau)$ correspond to the inflection points in the director profiles and evolve during the time τ . Figures 3(a) and 3(b) show the director orientation scenario: the effect of \mathbf{T}_p and \mathbf{T}_{tm} on the reorientation process is increased by the large external voltage $U_0 = 14$. This value of voltage causes a larger deformation near the inner cylinder than the other case $U_0 = 6$ [curves 1 to 5 in Fig. 3(b)]. The torque balance keeps the main role of $\mathbf{T}_{\text{elast}}$ and \mathbf{T}_{el} over the time interval $\tau < \tau_5$, near the inner cylinder. After the time period τ_5 , a quick growth of the negative profile occurs in the relaxation way [curves 6 to 8, Fig. 3(b)] and the negative part of the reorientation profile of director takes pi form [curve 10, in Fig. 3(b)]. A similar behavior is shown by the director reorientation due to the model of $\mathbf{P} = \mathbf{0}$ [Fig. 3(a)]. The new voltage is 2.5 times bigger than

the previous one; all processes are significantly speeded up, and the inflection points of the electric field [Figs. 5(a) and 5(b)] have not evolved. Director orientation in the nematic cavity, as plotted in Figs. 2(a) and 2(b), exhibits the inner planar orientation $n_r(r) = 0$, for $r = r_w$. The space position of planar director [Figs. 3(a) and 3(b)] can be classified as steady wall position versus the situation shown in Figs. 2(a) and 2(b), showing a moving wall, which in turn disappears at the τ_R [Figs. 2(a) and 2(b)]. We will return to the discussion of moving walls a little later, but in the meantime we will consider the evolution of both the velocity $u(r, \tau)$ and the temperature $\chi(r, \tau)$ fields.

We first investigate the electrically driven nematic flow in microfluidic homogeneously aligned liquid crystal capillary containing a temperature gradient $\nabla\chi$. The curves shown on the left-hand side in Fig. 6(a) correspond to the evolution of the dimensionless velocity $u(r, \tau_i)$, for different times $\tau_i = 0.01i$ ($i = 1, \dots, 7$) [$\tau_7 \equiv \tau_R$ ($t_R \sim 50$ ms)], to its equilibrium distribution across the HALC cavity $a < r < a + 1$, both under the effect of the electric field $U_0 = 6$ and the heat flux directed from the inner cooler $\chi_{\text{in}} = 0.97$ to the hotter outer $\chi_{\text{out}} = 0.9862$ restricted surfaces, without accounting the flexoelectric polarization ($\mathbf{P} = \mathbf{0}$) (case I), whereas the curves shown on the right-hand side in Fig. 6(b) correspond to the evolution of the dimensionless velocity $u(r, \tau_i)$ to its equi-

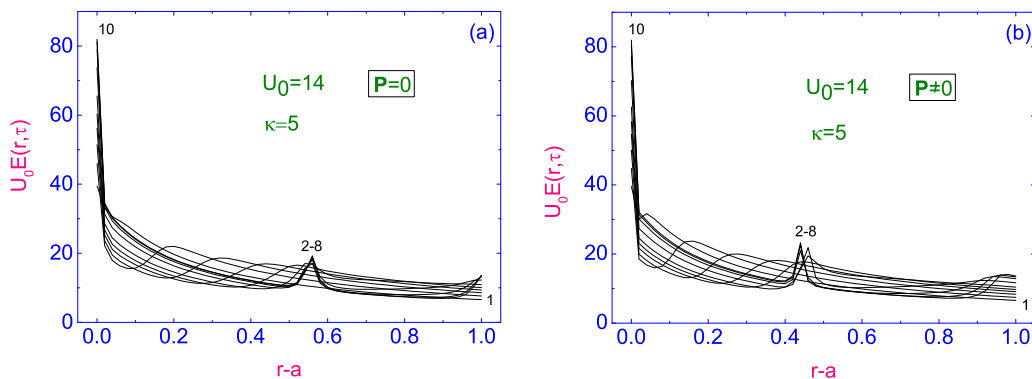


FIG. 5. Same as described in the caption Fig. 3, but a plot of the evolution of the electric field $U_0 E(r, \tau_i)$ to its equilibrium distribution $U_0 E^{\text{eq}}(r, \tau_{10}) \equiv U_0 E^{\text{eq}}(r)$ across the microsized HALC cavity $a \leq r \leq a + 1$, both for the cases $\mathbf{P} = \mathbf{0}$ (a) and $\mathbf{P} \neq \mathbf{0}$ (b), respectively. Here, $U_0 = 14$ and $\kappa = 1$.

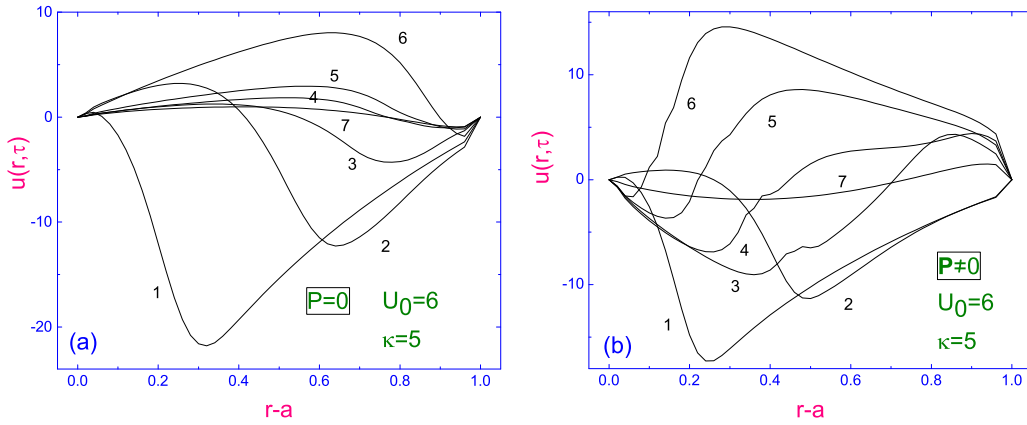


FIG. 6. Plot of the evolution of the velocity field $u(r, \tau_i)$ for different times $\tau_i = 0.01i$ ($i = 1, \dots, 7$) [$\tau_7 = \tau_R$ ($t_R \sim 50$ ms)], to its equilibrium distribution $u^{\text{eq}}(r, \tau_7) \equiv u^{\text{eq}}(r)$ across the microsized HALC cavity $a \leq r \leq a + 1$, both for the cases $\mathbf{P} = \mathbf{0}$ (a) and $\mathbf{P} \neq \mathbf{0}$ (b), respectively. Here, $U_0 = 6$ and $\kappa = 5$.

librium distribution across the HALC cavity with accounting the flexoelectric polarization ($\mathbf{P} \neq \mathbf{0}$) (case II), respectively. It is shown, based on our calculations, that accounting the flexoelectric effect leads to a change, compared to the case I, in the direction of the steady hydrodynamic flow $u^{\text{eq}}(r)$. Indeed, in the case I, the steady flow is directed in the positive sense as $\mathbf{v}^{\text{eq}}(r) = u^{\text{eq}}(r)\hat{\mathbf{e}}_z$, whereas in the case II, the steady hydrodynamic flow mostly is directed in the negative sense as $\mathbf{v}^{\text{eq}}(r) = -u^{\text{eq}}(r)\hat{\mathbf{e}}_z$, excluding a small area near the hotter outer restricted surface, where the flow is directed in the positive sense. Figures 7(a) and 7(b) show both the velocity field $u(r, \tau_i)$ [see Fig. 7(a)] and the dimensionless hydrodynamic pressure $Q(r, \tau_i)$ [see Fig. 7(b)] evolution, for different times $\tau_1 = 0.001$ (~ 0.7 ms), $\tau_2 = 0.025$ (~ 17.5 ms), $\tau_3 = 0.04$ (~ 28 ms), $\tau_4 = 0.05$ (~ 35 ms), $\tau_5 = 0.06$ (~ 42 ms), and [$\tau_6 = \tau_R = 0.15$ ($t_R \sim 0.1$ s)], to their equilibrium distributions $u^{\text{eq}}(r, \tau_6) \equiv u^{\text{eq}}(r)$ and $Q^{\text{eq}}(r, \tau_R) \equiv Q^{\text{eq}}(r)$ across the microsized HALC cavity $a \leq r \leq a + 1$, for the case $\mathbf{P} \neq \mathbf{0}$, and under the effect of the electric field $U_0 = 3.5$ and the temperature difference $\Delta\chi = 0.0162$. Our calculations show that in the early stage of the evolution process up to 17.5 ms [see curves 1 and 2, Fig. 7(a)], the excited velocity field

$u(r, \tau_i)$ ($\tau_i = 1, 2$) is still weak and the hydrodynamic flow is directed in the positive sense, excluding a small area near the cooler inner restricted surface. Further, with the growth of time, the excited velocity field $u(r, \tau_3)$ becomes large, especially in the vicinity of the outer cylinder, and, finally, the relaxation process is characterized by getting to the equilibrium distribution $u^{\text{eq}}(r, \tau_6) \equiv u^{\text{eq}}(r)$ across the LC cavity, after time [$\tau_6 = \tau_R = 0.15$ ($t_R \sim 0.1$ s)]. This distribution is characterized by the maximum value of the velocity $|u_{\text{max}}^{\text{eq}}| \sim 2.42$ (~ 34 $\mu\text{m/s}$) near the inner cylinder. Notice also that relaxation of the dimensionless hydrodynamic pressure $Q(r, \tau_i)$ to its equilibrium distribution across the HALC cavity exhibits a complex behavior. According to our calculations, the magnitude of $Q(r, \tau_i)$ exhibits minima close to both boundaries and a maximum near the inner cylinder, whose value is 3.18 (~ 0.32 pN/ μm) [see Fig. 7(b), curve 6].

Figures 8(a) and 8(b) address the effect of the radially applied electric field \mathbf{E} , for a number of values of U_0 ranging from 1.0 (curve 1) to 3.0 (curve 5), on the resulting equilibrium distributions of the velocity field $u^{\text{eq}}(r)$ across the microsized HALC cavity $a \leq r \leq a + 1$, for two cavity sizes $\kappa = 1$ (a) and $\kappa = 0.1$ (b), respectively. According

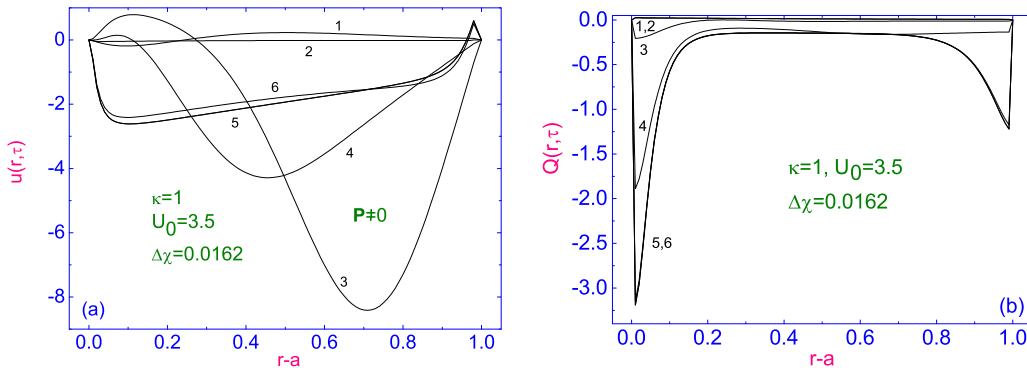


FIG. 7. Results of calculations of the space and time evolution for the dimensionless velocity field $u(r, \tau_i)$ (a) and the dimensionless hydrodynamic pressure $Q(r, \tau_i)$ (b), for different times $\tau_1 = 0.001$ (~ 0.7 ms), $\tau_2 = 0.025$ (~ 17.5 ms), $\tau_3 = 0.04$ (~ 28 ms), $\tau_4 = 0.05$ (~ 35 ms), $\tau_5 = 0.06$ (~ 42 ms), and [$\tau_6 = \tau_R = 0.15$ ($t_R \sim 0.1$ s)], to their equilibrium distributions $u^{\text{eq}}(r, \tau_6) \equiv u^{\text{eq}}(r)$ and $Q^{\text{eq}}(r, \tau_R) \equiv Q^{\text{eq}}(r)$ across the microsized HALC cavity $a \leq r \leq a + 1$, under the effect of the electric field $U_0 = 3.5$ and the temperature difference $\Delta\chi = 0.0162$. Here, $\mathbf{P} \neq \mathbf{0}$ and $\kappa = 1$.

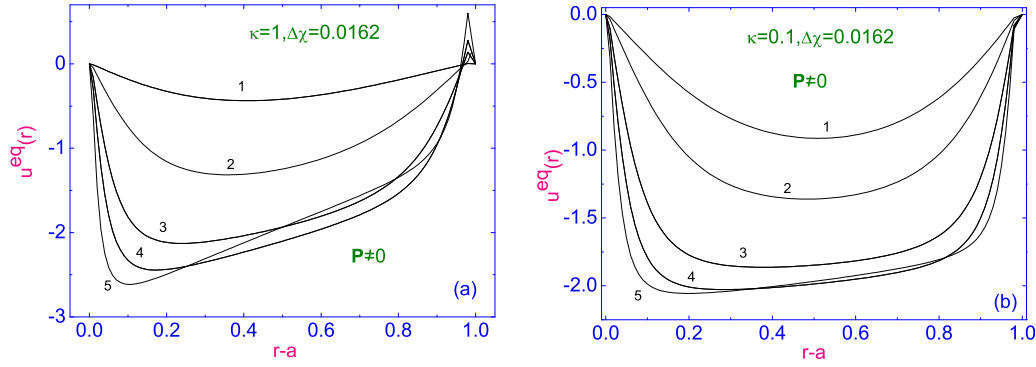


FIG. 8. Radial equilibrium distribution of the dimensionless velocity field $u^{\text{eq}}(r)$ across the micro-sized HALC cavity $a \leq r \leq a + 1$, for different values of the radially applied electric field: $U_0 = 1.0$ (curve 1), $U_0 = 1.1$ (curve 2), $U_0 = 1.5$ (curve 3), $U_0 = 2.0$ (curve 4), and $U_0 = 3.0$ (curve 5), respectively, for the case $\mathbf{P} \neq \mathbf{0}$. Here, $\kappa = 1$ (a) and $\kappa = 0.1$ (b), respectively.

to our calculations, when the temperature gradient is also present, \mathbf{E} produces a pronounced effect on the radial equilibrium distribution of the dimensionless velocity field $u^{\text{eq}}(r)$ across the micro-sized HALC cavity $a \leq r \leq a + 1$, whereas increasing the LC cavity size from $\kappa = 0.1$ to 1.0 produces a small increase in $u^{\text{eq}}(r)$ from $u_{\text{max}}^{\text{eq}}(U_0 = 3.0) \sim 2.0$ ($\sim 28.3 \mu\text{m/s}$) [see curve 5, Fig. 8(b)] to $u_{\text{max}}^{\text{eq}}(U_0 = 3.0) \sim 2.6$ ($\sim 36.5 \mu\text{m/s}$) [see curve 5, Fig. 8(a)], respectively.

Figure 9(a) shows the effect of U_0 on the maximum magnitude $u_{\text{max}}(U_0) \equiv u_{\text{max}}^{\text{eq}}(U_0)$ for different cavity sizes $\kappa = 1.0$ and 0.1. Our calculations have shown that the dependence of the maximum value of the absolute equilibrium velocity $|u_{\text{max}}(U_0)|$ on the value of electric field U_0 is characterized by the monotonic increase of $|u_{\text{max}}(U_0)|$ up to maximum value 2.6 ($\sim 35 \mu\text{m/s}$) at $U_0 = 3.0$, in the case $\kappa = 1$, and up to maximum value 2.0 ($\sim 28 \mu\text{m/s}$) at $U_0 = 3.0$, in the case $\kappa = 0.1$, respectively, whereas further increase of the value of U_0 leads to decrease in $|u_{\text{max}}(U_0)|$. Such behavior of $|u_{\text{max}}(U_0)|$ vs U_0 can be explained by the rapid growth of the coefficient $\delta_4(\pi U_0)^2$, in the left-hand part of Eq. (14), with the growth of U_0 . In this case, the contribution of electric forces prevails over the contributions of viscous, elastic, and thermomechanical forces, and when $U_0 \gg 1$, the evolution of the velocity

field $u(r, \tau)$ in the micro-sized HALC cavity is described by the reduced dimensionless Navier-Stokes equation [see Eq. (14)], which can be rewritten as [6]

$$\lim_{U_0 \rightarrow \infty} \delta_4(\pi U_0)^2 \dot{u}(r, \tau) \rightarrow \infty. \quad (22)$$

In the case when $U_0 \rightarrow \infty$, and with accounting the no-slip boundary condition [see Eq. (2)], one has that $\lim_{U_0 \rightarrow \infty} u(r, \tau) \rightarrow 0$, and any horizontal steady flow of the LC phase stops in the micro-sized HALC capillary, since under the influence of strong external electric field \mathbf{E} the dipoles of molecules forming the LC phase are oriented along this field. This once again shows that the macroscopic description of the nature of the hydrodynamic flow of an anisotropic liquid subtly senses the microscopic structure of the LC material.

The effect of curvature κ and the flexoelectric coupling on the maximum values of steady flow velocities $|u_{\text{max}}(\kappa)|$, calculated for the case $U_0 = 6$, is shown in Fig. 9(b). The difference between corresponding values $|u_{\text{max}}(\kappa)|$ is in the range of 25%, and the flow verse is opposite for the case $\mathbf{P} \neq \mathbf{0}$ relatively the case $\mathbf{P} = \mathbf{0}$. The second observation of the influence of the flexoelectric coupling on the steady flow is that the maximum of the velocity profile is fixed near the hot cylinder. The dimensional flow velocity $|u_{\text{max}}| \sim 10\text{--}20 \mu\text{m/s}$

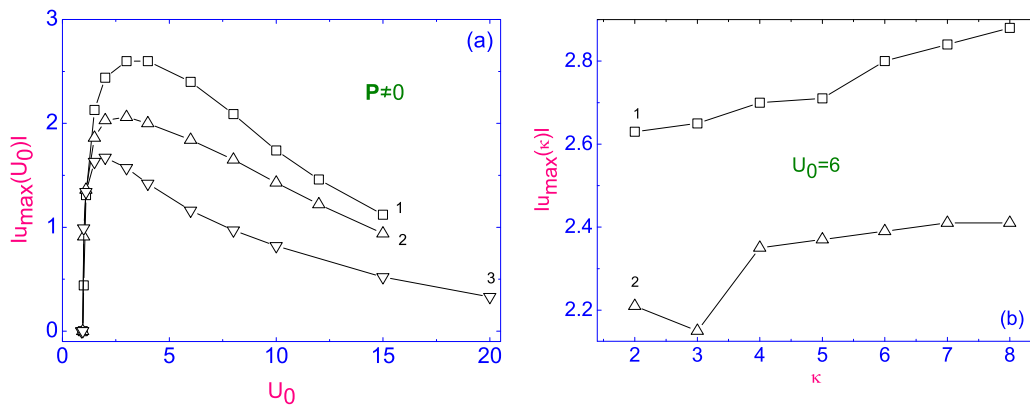


FIG. 9. (a) Dependence of $u_{\text{max}}(U_0) \equiv u_{\text{max}}^{\text{eq}}(U_0)$ vs U_0 for two sizes of the HALC cavity: $\kappa = 1$ (curve 1) and $\kappa = 0.1$ (curve 2), respectively, and for the case $\mathbf{P} \neq \mathbf{0}$, whereas the curve 3 shows the effect of U_0 on the maximum steady flow velocity, which is borrowed from Ref. [6] [see Fig. 8(b)]. (b) Effect of curvature κ and the flexoelectric coupling on the maximum values of steady flow velocities $|u_{\text{max}}(\kappa)|$. Results were obtained for $U_0 = 6$, $\Delta = 0.0162$, and for the models of $\mathbf{P} = \mathbf{0}$ (curve 1) and $\mathbf{P} \neq \mathbf{0}$ (curve 2), respectively.

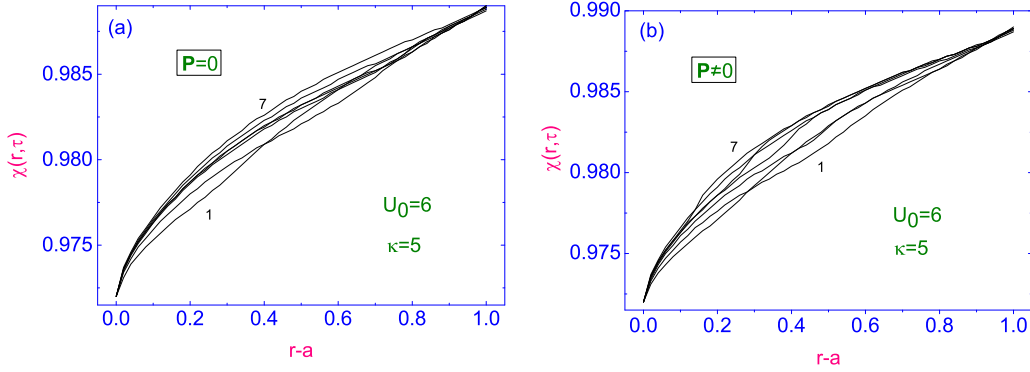


FIG. 10. Same as described in the caption of Fig. 2, but a plot of the evolution of the temperature field $\chi(r, \tau) = T(r, \tau)/T_{NI}$, for different times $\tau_i = 0.01i$ ($i = 1, \dots, 7$) [$\tau_7 = \tau_R$ ($t_R \sim 50$ ms)], to its equilibrium distribution $\chi^{eq}(r, \tau) \equiv \chi^{eq}(r)$ across the microsized HALC cavity $a \leq r \leq a + 1$, both for the cases $\mathbf{P} = \mathbf{0}$ (a) and $\mathbf{P} \neq \mathbf{0}$ (b), respectively. Here, $U_0 = 6$.

in Fig. 9(b) is of the same order as found in the experimental observation of mechanical pumping reported in Ref. [29].

The evolution of the dimensionless temperature field $\chi(r, \tau) = T(r, \tau)/T_{NI}$ to its equilibrium distribution $\chi(r, \tau_R)$ across the microsized HALC cavity, both in the cases I and II, at different times $\tau_i = 0.01i$ ($i = 1, \dots, 7$) ($\tau_7 = \tau_R$) ($t_R \sim 50$ ms), are shown in Figs. 10(a) and 10(b), respectively. In both cases I and II, we have a weak nonlinear distribution of the temperature field $\chi^{eq}(r)$ across the microsized HALC cavity.

As noted above, in some cases, for the model of $\mathbf{P} \neq \mathbf{0}$ and $U_0 = 6$, the relaxation regime for the orientational dynamics of the director's field component $n_r(r, \tau)$ to its equilibrium distribution $n_r^{eq}(r)$ allows the formation of the kinklike wave, which is spreading across the microsized HALC cavity $a \leq r \leq r + a$ [see curves from 4 to 7, Fig. 2(b)]. If so, it probably can be observed in polarized white light. Taking into account that the director reorientation takes place in the narrow area of the nematic 5CB sample (the width of the kinklike wave) under influence of the voltage $U_0 = 6$, applied between two horizontal coaxial cylinders, the kinklike wave can be visualized in polarized white light as a dark strip running across the microsized HALC cavity. Having obtained the steady wall position $r_w(\tau)$, where the director component $n_r(r)$ is equal to 0, one can calculate the velocity $u_w(\tau) = r_w/\tau$ of wall prop-

agation across the microsized LC cavity. Figure 11 shows the influence of curvature κ on the steady wall position $r_w(\tau)$ and velocity $u_w(\tau)$ vs τ across the HALC cavity $a \leq r \leq a + 1$, for the case $\mathbf{P} \neq \mathbf{0}$ and under the effect of $U_0 = 6$ and $\Delta\chi = 0.0162$. The decreasing of curvature κ shifts the time dependence of $r_w(\tau)$ and $u_w(\tau)$, and maintains similarity in the main kinetic features of these quantities. Figure 11(a) shows the uniform motion of the wall out of initiation time period. From the data in Fig. 11(a), the velocity of wall propagation along the radial coordinate, from outer to inner cylinder, can be estimated as $u_w = 10$, which is of about three times of the maximum horizontal speed $|u_{\max}(U_0 = 6, \kappa = 5)| \sim 2.7$. Figure 11(b) shows the oscillating horizontal steady wall motion. The oscillation symmetry is broken near the inner cell boundary, and this fact can be explained by the process of kink dilution.

Notes that the relaxation behavior of the director field $\hat{\mathbf{n}}$ in the form of the kinklike distortion wave spreading along the normal to both cylindrical boundaries probably can be observed in polarized white light. Taking into account that the director reorientation takes place in the narrow area of the LC sample (the width of the kinklike distortion wave), as shown in Fig. 2(b), under applied voltage U_0 , for instance, $U_0 = 6$ in the 5CB cavity size in $a \leq r \leq a + 1$, where $a = R_1/(R_1 + R_2) = 0.2$, the kinklike distortion wave can be vi-

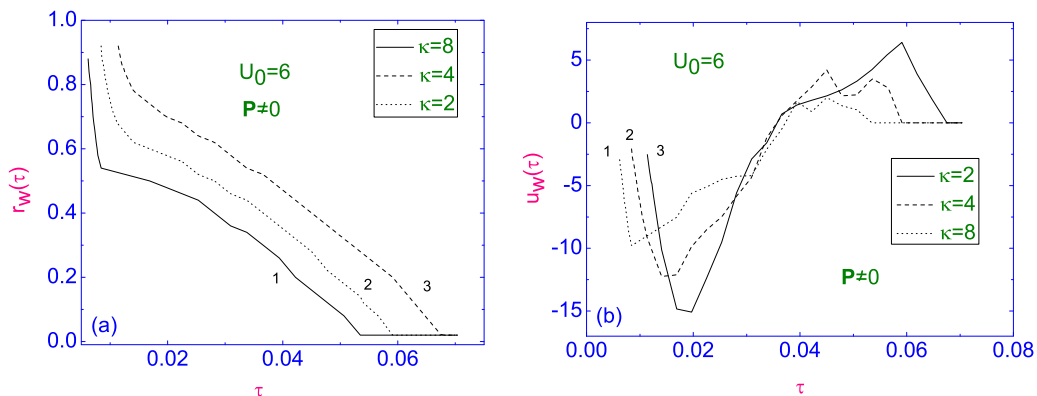


FIG. 11. Plot of the evolution of the wall horizontal position $r_w(\tau)$ (a) and velocity $u_w(\tau)$ (b) vs τ across the HALC cavity $a \leq r \leq a + 1$, for the case $\mathbf{P} \neq \mathbf{0}$ and under the effect of $U_0 = 6$ and $\Delta\chi = 0.0162$. Results were obtained for $\kappa = 8$ (curves 1), 4 (curves 2), and 2 (curves 3), respectively.

sualized in polarized white light as a dark strip running along the normal to both cylindrical boundaries, with the velocity $v \sim 10\text{--}20 \mu\text{m/s}$.

IV. CONCLUSION

An electrically driven fluid pumping principle and a mechanism of kinklike distortion of the director field $\hat{\mathbf{n}}$ in a microfluidic homogeneously aligned liquid crystal (HALC) channel, confined between two infinitely long horizontal coaxial cylinders subjected to both a temperature gradient ∇T and radially applied electric field \mathbf{E} , has been proposed. Both the fluid pumping principle and the kinklike distortion mechanism are based on the coupling between the electric \mathbf{E} and director $\hat{\mathbf{n}}$ fields, together with accounting both the effect of the temperature gradient ∇T and the flexoelectric polarization \mathbf{P} . In the nematic microfluidic channel where director anchoring on the bounding surfaces is the same, i.e., both homogeneous, and when the gradient of the temperature field ∇T does not exist, the horizontal flow of the nematic material is excited only by the radially applied electric field $\mathbf{E}(r) = E(r)\hat{\mathbf{e}}_r$. In turn, accounting both the temperature gradient ∇T and the flexoelectric polarization \mathbf{P} leads to the additional contributions both to the torque and linear momentum balance equations. Calculations, based upon the nonlinear extension of the classical Ericksen-Leslie theory, with accounting the entropy balance equation, show that due to the coupling among the ∇T , $\nabla\hat{\mathbf{n}}$, \mathbf{P} , and \mathbf{E} in the HALC microfluidic channel the kinklike distortion wave spreading along normal to both cylindrical boundaries may be excited. Calculations show that the resemblance to the kinklike distortion wave depends on the value of radially applied electric field \mathbf{E} and the curvature of these boundaries. Our calculations also show that, under the effect of the named flexoelectric perturbations and at high curvature of the inner cylinder, the HALC microvolume settles down to a nonstandard relaxation mechanism and a nonstandard flow regime $u^{\text{eq}}(r)\hat{\mathbf{e}}_z$ in the horizontal direction. We worked out the conditions (in terms of curvature κ and voltage U_0) producing a relaxation mechanism of the double π form, with an intermediate relaxation wall (steady wall motion has been extensively studied in spintronics, see Refs. [29,30]). In the range of radii $R_2/R_1 > 2$ and voltage $U \sim 5.3\text{--}8.5$ V, the maximum of the stationary flow velocity $u_{\text{max}}^{\text{eq}}$ is found near the hot outer cylinder. Higher voltages block up the relaxation mechanism, and the maximum flow decreases. In the case when the voltage $U_0 \rightarrow \infty$, one has that $\lim_{U_0 \rightarrow \infty} u(r, \tau) \rightarrow 0$, and any horizontal steady flow $\mathbf{v}(r, t) = v_z(r, t)\hat{\mathbf{e}}_z = u(r, t)\hat{\mathbf{e}}_z$ of the LC phase stops in the microsized HALC capillary, since under the influence of strong external electric field \mathbf{E} the dipoles of molecules forming the LC phase are oriented along this field. This once again shows that the macroscopic description of the nature of the hydrodynamic flow of an anisotropic liquid subtly senses the microscopic structure of the LC material. Further comparison between the two treatments shows that allowing for flexoelectric coupling increases the maximum of the stationary flow velocity $u_{\text{max}}^{\text{eq}}$ by some 25%. So, our calculations show that the most pronounced effect of flexoelectricity in the microvolume HALC cavity between two coaxial cylinders is observed on the orientational dynamics and weak effect on the

flow velocity. Calculated flow velocity is of the same order as found in the experimental observation of mechanical pumping reported in [28].

Our calculations also show, on the one hand, that, under certain conditions, in terms of curvature of cylinders κ and the voltage U , applied between cylinders, the torques and forces acting on the director $\hat{\mathbf{n}}$ may excite the kinklike distortion wave spreading along the normal to both cylindrical boundaries, whose resemblance to a kinklike distortion wave depends on the value of U and the curvature of the inner cylinder. It has been worked out, on the other hand, the conditions, in terms of κ and U , producing the distortion mechanism of the $\hat{\mathbf{n}}$ in the double π form, with the intermediate relaxation wall.

Note that the relaxation behavior of the director field $\hat{\mathbf{n}}$ is observed in the form of the kinklike wave $n_r(r, t)$ which is spreading across the HALC cavity, it probably can be observed in polarized white light. Taking into account that the director reorientation takes place in the narrow area of the nematic 5CB sample (the width of the kinklike wave) under influence of the voltage $U_0 = 6$, applied between two horizontal coaxial cylinders, the kinklike wave can be visualized in polarized white light as a dark strip running across the microsized HALC cavity. This once again shows that the macroscopic description of the nature of the hydrodynamic flow of an anisotropic liquid subtly senses the microscopic structure of the LC material.

We believe that the present investigation can shed some light on the problem of precise handling of microvolume LC drops, which requires self-contained micropumps.

ACKNOWLEDGMENT

This study was funded by RFBR and DFG, Project No. 20-52-12040 and by the Ministry of Education and Science of the Russian Federation (Grant No. FSFZ-2020-0019).

APPENDIX: HYDRODYNAMIC EQUATIONS WITH ACCOUNTING FOR THE ELECTRIC FIELD AND THE TEMPERATURE GRADIENT

For two component director $\hat{\mathbf{n}} = n_r\hat{\mathbf{e}}_r + n_z\hat{\mathbf{e}}_z$ in a cylindrical coordinate, both the elastic and electric energy densities are given by dimension forms $2\mathcal{W}_F = K_1 n_{r,r}^2 + K_3 n_{z,r}^2$ and $2\psi^{el} = \epsilon_0(\epsilon_{\perp} + \epsilon_a n_r^2)E^2(r) + 2P_r E(r)$, respectively, whereas the viscous, thermomechanical, and thermal parts of the full dissipation function of nematic are given by dimension forms: $2\mathcal{R}_{\text{vis}} = \gamma_1(n_r^2 + n_z^2) + v_{z,r}(\dot{n}_r n_z - \dot{n}_z n_r)[\gamma_1 + \gamma_2(n_z^2 - n_r^2)] + \mathcal{H}v_{z,r}^2$, $\mathcal{R}_{\text{tm}} = \xi T_r[(\frac{1}{2} + n_z^2)(\dot{n}_r n_{r,r} + \dot{n}_z n_{z,r}) + \frac{1}{2r} n_r n_z (\dot{n}_z n_r - \dot{n}_r n_z)] + v_{z,r} \xi T_r [n_{r,r}(n_z + \frac{1}{4} n_z n_r^2) - \frac{3}{4r} n_z n_r]$, and $\mathcal{R}_{\text{th}} = \frac{T_r^2}{2T}(\lambda_{\parallel} n_r^2 + \lambda_{\perp} n_z^2)$, respectively. Here, $2\mathcal{H} = \alpha_4 + \frac{1}{2}(\alpha_5 + \alpha_6 + \gamma_1) + \alpha_1 n_r^2 n_z^2 + \gamma_2 n_z^2 - n_r^2$ is the hydrodynamic function, $\mathbf{v} = v_z \hat{\mathbf{e}}_z$, $v_{z,r}$ is the unique nonzero component of the tensor $\nabla\hat{\mathbf{v}}$, $\dot{n}_x = n_{x,t} = \partial n_x / \partial t$ ($x = r, z$), and $n_{r,r}$, n_r/r and $n_{z,r}$ are the components of the distortion $\nabla\hat{\mathbf{n}}$.

The linear moment balance equation has the form

$$\rho\dot{\mathbf{v}} = \nabla \cdot \boldsymbol{\sigma} + \nabla\psi^{el}, \quad (\text{A1})$$

where ρ is the density of nematic phase, $\sigma = \frac{\delta \mathcal{R}}{\delta \nabla \mathbf{v}}$ is the stress tensor. The nonzero elastic stress components are defined by the elastic energy density as $\sigma_{rr}^{\text{elast}} = -[Q + n_{r,r}(\partial \mathcal{W}_F / \partial n_{r,r}) + n_{z,r}(\partial \mathcal{W}_F / \partial n_{z,r})]$ and $\sigma_{\alpha\alpha}^{\text{elast}} = -\{Q + (n_r/r)[\partial \mathcal{W}_F / \partial (n_r/r)]\}$. The nonelastic component is the shear stress $\sigma_{rz} = \partial \mathcal{R} / \partial v_{z,r}$. Equation (A1) has the dimensionless form as Eqs. (14) and (15). Equation (14) is approximated by Eq. (19) due to $\delta_4 \ll 1$, and Eq. (21) for pressure Q is the first integral of Eq. (15).

The heat conduction equation has the form

$$\rho C_p \dot{T} = -\nabla_r q_r, \quad (\text{A2})$$

where C_p is the heat capacity, $q_r = -T(\delta \mathcal{R} / \delta T_{,r})$ denotes the heat flux component. The expression for the radial heat flux is $q_r = T_r(\lambda_{\parallel} n_r^2 + \lambda_{\perp} n_z^2) + \xi T[(\frac{1}{2} + n_z^2)(\dot{n}_r n_{r,r} + \dot{n}_z n_{z,r}) + \frac{1}{2r} n_r n_z (\dot{n}_z n_r - \dot{n}_r n_z)] + v_{z,r} \xi T[n_{r,r}(n_z + \frac{1}{4} n_z n_r^2) - \frac{3}{4r} n_z n_r]$. The full heat conductivity equation has the dimensionless form

$$\begin{aligned} (\pi U_0)^2 \delta_5 \dot{\chi} = & \nabla_r \left[\chi_{,r} (\lambda n_r^2 + n_z^2) + \delta_6 \chi \left(\frac{1}{2} + n_z^2 \right) (\dot{n}_r n_{r,r} + \dot{n}_z n_{z,r}) \right] \\ & + \delta_6 \nabla_r \left\{ \chi \frac{1}{2r} n_r n_z (\dot{n}_z n_r - \dot{n}_r n_z) + u_{,r} \left[n_{r,r} \left(n_z + \frac{1}{4} n_z n_r^2 \right) - \frac{3}{4r} n_z n_r \right] \right\}, \end{aligned} \quad (\text{A3})$$

where $\delta_6 = \xi(K_1/\lambda_{\perp} \gamma_1 d^2)$ and $\lambda = \lambda_{\parallel}/\lambda_{\perp}$. The parameter $\delta_6 = \delta_2/\delta_3 \ll 1$ for nematics and Eq. (A3) has the form (18). The quasistationary form of the solution of the equation with $\delta_5 \ll 1$ and $\delta_6 \ll 1$ is Eq. (20).

-
- [1] R. B. Schoch, J. Han, and P. Renaud, *Rev. Mod. Phys.* **80**, 839 (2008).
- [2] M. Rauscher and S. Dietrich, *Annu. Rev. Mater. Res.* **38**, 143 (2008).
- [3] A. D. Rey, *Soft Matter* **6**, 3402 (2010).
- [4] W. Sparreboom, A. van den Berg, and J. C. T. Eijkel, *New J. Phys.* **12**, 015004 (2010).
- [5] A. V. Zakharov and A. A. Vakulenko, *J. Chem. Phys.* **127**, 084907 (2007).
- [6] A. V. Zakharov, P. V. Maslennikov, and S. V. Pasechnik, *Phys. Rev. E* **101**, 062702 (2020).
- [7] J. G. Cuennet, A. E. Vasdekis, L. De Sio, and D. Psalis, *Nat. Photonics* **5**, 234 (2011).
- [8] A. V. Zakharov and P. V. Maslennikov, *Phys. Rev. E* **96**, 052705 (2017).
- [9] A. J. Pascall and T. M. Squires, *Lab Chip* **10**, 2350 (2010).
- [10] T. M. Squares and S. R. Quake, *Rev. Mod. Phys.* **77**, 977 (2005).
- [11] P. G. de Gennes and J. Prost, *The Physics of Liquid Crystals*, 2nd. ed. (Oxford University Press, Oxford, 1995).
- [12] A. A. Vakulenko and A. V. Zakharov, *Phys. Rev. E* **88**, 022505 (2013).
- [13] R. B. Meyer, *Phys. Rev. Lett.* **22**, 918 (1969).
- [14] J. L. Ericksen, *Arch. Ration. Mech. Anal.* **4**, 231 (1960).
- [15] F. M. Leslie, *Arch. Ration. Mech. Anal.* **28**, 265 (1968).
- [16] L. D. Landau and E. M. Lifshitz, *Fluid Mechanics* (Pergamon, Oxford, 1987).
- [17] C. V. Brown and N. J. Mottram, *Phys. Rev. E* **68**, 031702 (2003).
- [18] M. Marinelli, A. K. Ghosh, and F. Mercuri, *Phys. Rev. E* **63**, 061713 (2001).
- [19] N. V. Madhusudana and R. B. Ratibha, *Mol. Cryst. Liq. Cryst.* **89**, 249 (1982).
- [20] P. Jamee, G. Pitsi, and J. Thoen, *Phys. Rev. E* **66**, 021707 (2002).
- [21] A. G. Chmielewski, *Mol. Cryst. Liq. Cryst.* **132**, 339 (1986).
- [22] A. V. Zakharov and A. A. Vakulenko, *Crystallogr. Rep.* **48**, 686 (2003).
- [23] I. W. Stewart, *The Static and Dynamic Continuum Theory of Liquid Crystals* (Taylor and Francis, London, 2004).
- [24] A. V. Zakharov and A. A. Vakulenko, *Phys. Rev. E* **80**, 031708 (2009).
- [25] S. R. de Groot and P. Masur, *Non-Equilibrium Thermodynamics* (Dover, New York, 1984).
- [26] I. S. Berezin and N. P. Zhidkov, *Computing Methods*, 4th ed. (Pergamon, Oxford, 1965).
- [27] L. Z. Ruan and J. R. Sambles, *Appl. Phys. Lett.* **86**, 052502 (2005).
- [28] S. A. Jewell, S. L. Cornford, F. Yang, P. S. Cann, and J. R. Sambles, *Phys. Rev. E* **80**, 041706 (2009).
- [29] A. Yamaguchi, T. Ono, S. Nasu, K. Miyake, K. Mibu, and T. Shinjo, *Phys. Rev. Lett.* **92**, 077205 (2004).
- [30] P. J. Metaxas, J. P. Jamet, A. Mougouin, M. Cormier, J. Ferré, V. Baltz, B. Rodmacq, B. Dieny, and R. L. Stamps, *Phys. Rev. Lett.* **99**, 217208 (2007).